Wetting of rough surfaces in a phase field model

Jana Wolf[1,*]**, Yannic Flieger**[1]**, Felix Diewald**[2]**, Kai Langenbach**[3]**, Simon Stephan**[4]**, Hans Hasse**[4]**, and Ralf Müller**[5]

[1] Institute of Applied Mechanics, University of Kaiserslautern, 67663 Kaiserslautern, Germany

[2] Department of Optimization, Fraunhofer ITWM, 67663 Kaiserslautern, Germany

[3] Thermal Separation Science (endowed professorship of the state tyrol), University of Innsbruck, 6020 Innsbruck, Austria

[4] Laboratory of Engineering Thermodynamics, University of Kaiserslautern, 67663 Kaiserslautern, Germany

[5] Institute for Continuum Mechanics, Technical University of Darmstadt, 64287 Darmstadt, Germany

Surface wetting can be simulated using a phase field approach which describes the continuous liquid-gas transition with the help of an order parameter. In this publication, wetting of non-planar surfaces is investigated based on a phase field model by Diewald et al. [1,2]. Different scenarios of droplets on rough surfaces are simulated. The static equilibrium for those scenarios is calculated using an Allen-Cahn evolution equation. The influence of the surface morphology on the resulting contact angle is investigated while the width of the phase transition from liquid to gas is varied as a model parameter.

1 Introduction

Recently, there haven been considerable developments in manufacturing processes on small scales and as a result, techniques like micro milling, micro grinding or micro 3D printing become more and more evolved [3–6]. These techniques potentially allow for the control of surface properties via targeted modifications of the micromorphology.

The wetting behavior represents one important class of those surface properties. For many engineering applications, such as microfluidic devices, heat transfer, self-cleaning surfaces, etc., it is crucial to understand wetting phenomena. Thus, there is a need for models which can predict surface wetting, especially at small scales. As real technical surfaces always differ from ideal, perfectly smooth geometries, it is important that such models can deal with the impact of surface roughness.

Wetting can be modeled on an atomistic scale with the help of molecular dynamics (MD) [7,8]. On a larger scale, continuum models can be applied. They can be classified into sharp interface models and phase field (PF) models [9, 10]. In PF models, the interface between the fluid and the liquid phase is diffuse, which avoids discontinuities. As introduced in [2], PF models can be tied to MD models via an equation of state. An additional widening of the interphase transition allows for the model in [11] to bridge the gap between the atomistic scale and the scale of real microsurfaces. However, this is based on the assumption that the relevant wetting behavior is independent of the interface width as long as the surface energy remains unchanged.

This work focuses on a simple PF model. Simulations on rough surfaces are carried out in order to determine whether the results depend on the chosen interface width.

2 Phase field model

In this work, the phase field model from [1] is used to describe surface wetting. The model uses an order parameter φ which is defined such that $\varphi = 0$ in the gas phase and $\varphi = 1$ in the liquid phase. The order parameter can be seen as a normalized density, expressed as

$$\varphi = \frac{\rho - \rho''}{\rho' - \rho''} \,, \tag{1}$$

where ρ' is the density of the liquid phase and ρ'' is the density of the gas phase. Based on that order parameter, a free energy functional F is defined as follows:

$$F = \int_{\Omega} \left[12 \frac{\gamma_{\text{lv}}}{l} f(\varphi) + \frac{3}{4} \gamma_{\text{lv}} l |\nabla \varphi|^2 \right] \mathrm{d}V + \lambda \int_{\Omega} [\varphi - \varphi_0] \mathrm{d}V + \int_{\partial \Omega} [h(\varphi)\gamma_{\text{sl}} + (1 - h(\varphi))\gamma_{\text{sv}}] \, \mathrm{d}S \,, \tag{2}$$

where $f(\varphi)$ is the double well potential

$$f(\varphi) = \varphi^2(1 - \varphi)^2 \tag{3}$$

and $h(\varphi)$ is an interpolation function with

$$h(\varphi) = \varphi^3 \left(6\varphi^2 - 15\varphi + 10 \right) . \tag{4}$$

---

* Corresponding author: e-mail wolfj@rhrk.uni-kl.de, phone +49 631 205 2129

PAMM · Proc. Appl. Math. Mech. 2022;**22**:1 e202200275.   www.gamm-proceedings.com   **1 of 6**

https://doi.org/10.1002/pamm.202200275   © 2023 The Authors. *Proceedings in Applied Mathematics & Mechanics* published by Wiley-VCH GmbH.

In (2), γ_{lv}, γ_{sl} and γ_{sv} are the liquid-vapor, solid-liquid, and solid-vapor surface tensions, respectively, l is the width of the interface between liquid and vapor, and λ is a Lagrange multiplier. In this equation, the first integral describes the free energy in the bulk phase in the absence of solid surfaces. The factors of $12\frac{\gamma_{lv}}{l}$ in front of the double well potential and $\frac{3}{4}\gamma_{lv}l$ in front of the gradient term are chosen to assure that the energy of the interface stays consistent with the surface tension when the interface width is changed (for further details, c.f. [11]). The second integral in (2) constraints the mass via the Lagrange multiplier λ. The third integral is a surface integral over all solid boundaries of the domain Ω. It accounts for the surface energy as a part of the total energy of the domain. The interpolation function in (4) is chosen to assure that this surface energy is equal to the solid-liquid surface tension γ_{sl}, where the liquid phase is in contact with the surface and to the solid-vapor surface tension γ_{sv} where the gas is in contact with the surface [9]. The relation between the surface tensions and the contact angle of the droplet is established in section 4.

The finite element method is used to calculate an equilibrium state of the system. Therefore, the variation of the potential from (2) can be used to formulate the static equilibrium condition

$$\delta_\varphi F = 0 \,. \tag{5}$$

An Allen-Cahn evolution equation

$$\frac{\partial \varphi}{\partial t} = -M\delta_\varphi F \,, \tag{6}$$

with a pseudo time t and a mobility M, is used to come sufficiently close to the static solution so that (5) can be solved directly in a final nonlinear solution step.

3 Roughness model

The roughness of the surface is modeled as a Gaussian random distribution of the height y. Analogously to [12], a standard deviation of $\sigma = 0.8Ra$ is chosen to mimic a Gaussian surface. In x-direction, an equally spaced distribution of points is chosen. Clearly, this roughness model is rudimentary. Its objective is not to represent any real surface, but rather to lay the foundation for an investigation of the behavior of the phase field model on non-smooth surfaces.

4 Definition of contact angles on rough surfaces

The wettability of a surface is often described by the angle that forms between the liquid-vapor and the liquid-solid interface, referred to as the contact angle θ. The theoretical contact angle of a perfectly smooth surface can be calculated using Young's equation,

$$\cos\theta_{theo} = \frac{\gamma_{sv} - \gamma_{sl}}{\gamma_{lv}} \,, \tag{7}$$

where γ_{sv}, γ_{sl} and γ_{lv} are the surface tensions of the solid-vapor, solid-liquid, and liquid-vapor interface, respectively. The relation between surface tensions and contact angle results from the force balance at the contact line and is illustrated in Fig. 1.

On a rough surface, the interpretation of the term "contact angle" is less straightforward. Two possible definitions intuitively occur:

- the angle θ_{exp} between the liquid-vapor interface and the horizontal,

- the angle θ_{local} between the liquid-vapor interface and the local surface orientation.

In experiments, θ_{exp} is generally measured [13], whereas in simulations, both angles are accessible. In the context of this work, both θ_{exp} and θ_{local} are measured in the simulation results. Fig. 2 shows an example of both contact angle interpretations for a droplet on a rough surface.

5 Numerical examples

The aim of this study is to investigate the influence of the interface width on the resulting contact angles in the static equilibrium of a droplet. Therefore, a parameter study with two different roughness values Ra, 5 different theoretical contact angles θ_{theo} and three distinct values for the interface width l is carried out. For each value of Ra, four randomly generated surface geometries are used. The surfaces with $Ra = 0.1$ will be labeled "smooth" whereas the surfaces with $Ra = 1$ will be referred to as "rough" in the following analysis. An overview of the parameter study is given in Tab. 1.

All simulations start with an initial droplet of the same size. It is initialized via a $\tanh$-profile φ_0 for the order parameter

$$\varphi_0(r) = -\frac{1}{2}\left[\tanh\left(\frac{2}{l}(r-r_0)\right) + 1\right] + 1 \,, \tag{8}$$

PAMM · Proc. Appl. Math. Mech. **22**:1 (2022)
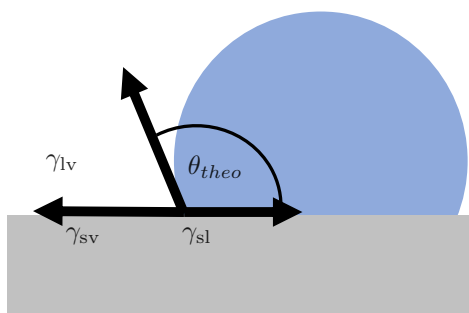
3 of 6

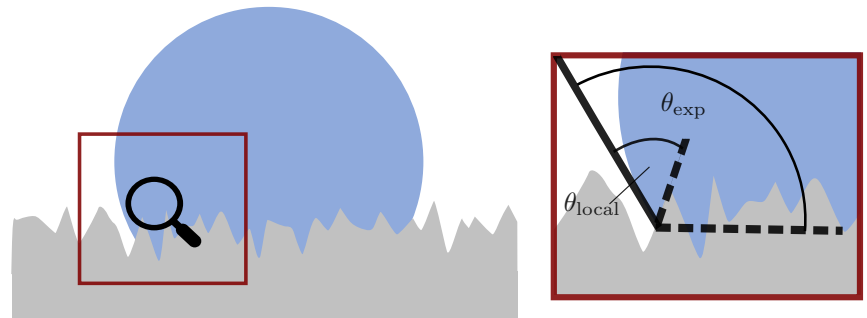**Fig. 1:** Relation between surface tensions and contact angle.

Fig. 2: Possible definitions of contact angles on a rough surface.

Table 1: Parameter study.

Ra	random seed for surface generation	θ_{theo}	l
0.1 "smooth"	2	30°	0.5
1 "rough"	17	78°	1.5
	105	90°	4.5
	398	120°	
		150°	

where r is the distance from the droplet center and $r_0 = 11$ is the radius of the initial droplet. The distance between the points in x-direction is 0.6. Linear, triangular finite elements for φ are used to discretize the domain. The discretization is chosen such that at least five elements resolve the liquid-vapor interface for the smallest interface width $l = 0.5$.

Two illustrative examples from the simulation results are chosen to qualitatively show the influence of the interface width, see Fig. 3, where l increases from top to bottom. On the left, a theoretical contact angle of $\theta_{\text{theo}} = 150°$ in combination with a smooth surface results in a sessile droplet for a small and middle interface width, whereas complete dewetting can be observed for a larger interface width. On the right, a theoretical contact angle of $\theta_{\text{theo}} = 30°$ on a rough surface leads to a sessile droplet for all values of l, but the spreading of the droplet substantially increases with the interface width l. Altogether, it is clearly visible from the illustration that the resulting wetting behavior is not independent from the interface width.
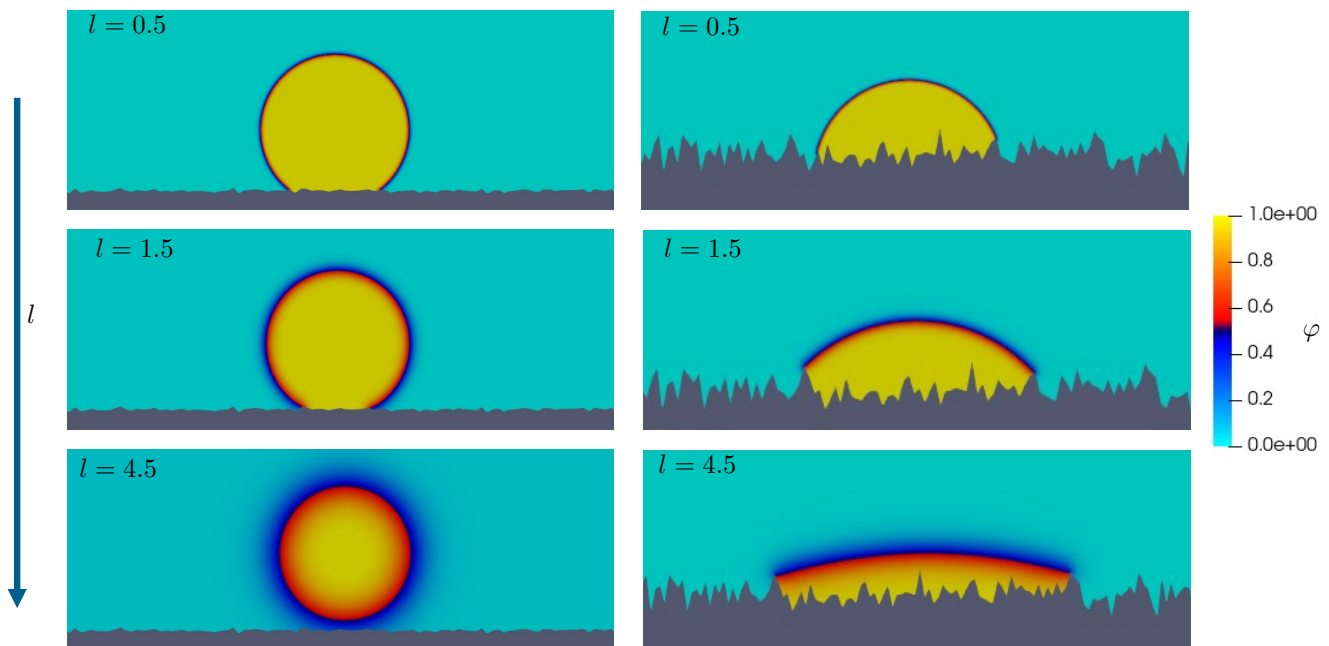

Fig. 3: Examples for the influence of the interface width l on the results. Left: $Ra = 0.1$, $\theta_{\text{theo}} = 150°$, right: $Ra = 1$, $\theta_{\text{theo}} = 30°$. l increasing from top to bottom.

A quantitative analysis of the parameter study is shown in Fig. 4 and 5. The four subfigures show the resulting contact angles θ_{exp} and θ_{local} for the four theoretical contact angles $\theta_{\text{theo}} = 30°$, 78°, 90°, and 120°, indicated by the grey dashed

line. The results for $\theta_{\text{theo}} = 150°$ are not shown here as the occuring complete dewetting, depicted in Fig. 3, does not allow for automatic contact angle measurement. In each subfigure, the results for the smooth surface are shown on the left and those for the rough surface on the right. The different colors indicate different values for the interface width and different symbols are used to differentiate between θ_{exp} and θ_{local}. For each case, 8 results are compared : 4 different random surfaces with the same settings, but different random seeds, where generated and in each simulation result, two contact angles can be measured (at the left and at the right side of the droplet). Fig. 4 shows the scatter of the results and Fig. 5 the mean values with a bar that represents the minimal value and the maximal value.
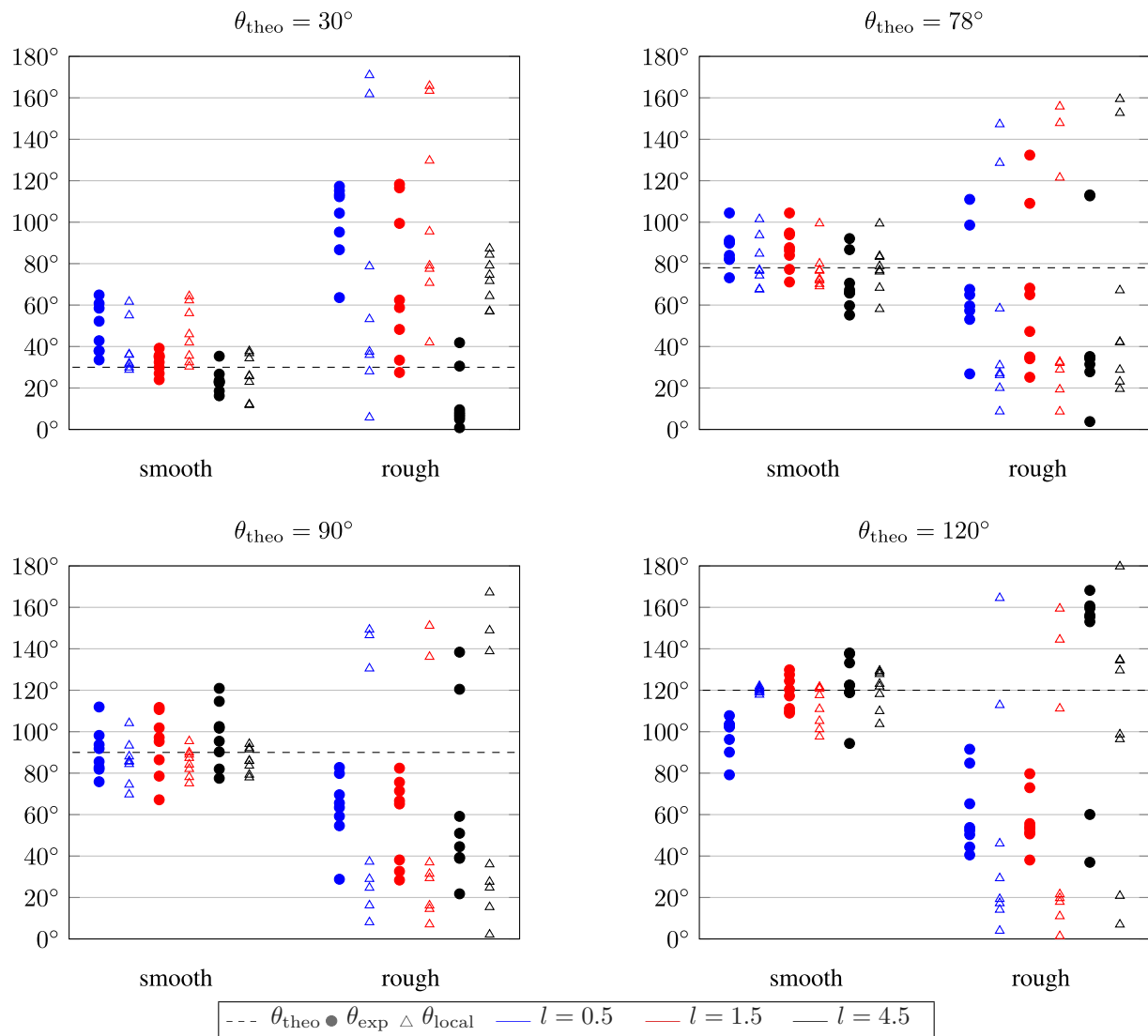

Fig. 4: Resulting contact angles θ_{exp} and θ_{local} for simulations with the parameters from Tab. 1.

It is visible from Fig. 4 and 5 that the scatter of the results is very large. This is especially the case for the rough surfaces. In general, the results for the smooth surfaces are closer to the theoretical contact angle. These observations hold for both θ_{exp} and θ_{local}. This is not surprising because this surface is closer to the perfectly smooth surface for which the theoretical contact angle is the expected result. However, the scattered results do not allow for any further assertions. No clear tendencies can be established, neither for the difference between θ_{exp} and θ_{local}, nor for the influence of the interface width. The reason for this behavior partially lies in the randomness of the surface profiles which results in a scattered distribution of the results. Additionally, the different relevant length scales (the droplet radius r_0, the interface width l and the surface roughness Ra) were chosen close to each other in this study and an interference between those scales is anticipated. Further research is therefore needed to establish the limits for l in relation to r_0 and Ra in which the droplet behavior can be regarded as independent of the interface width.
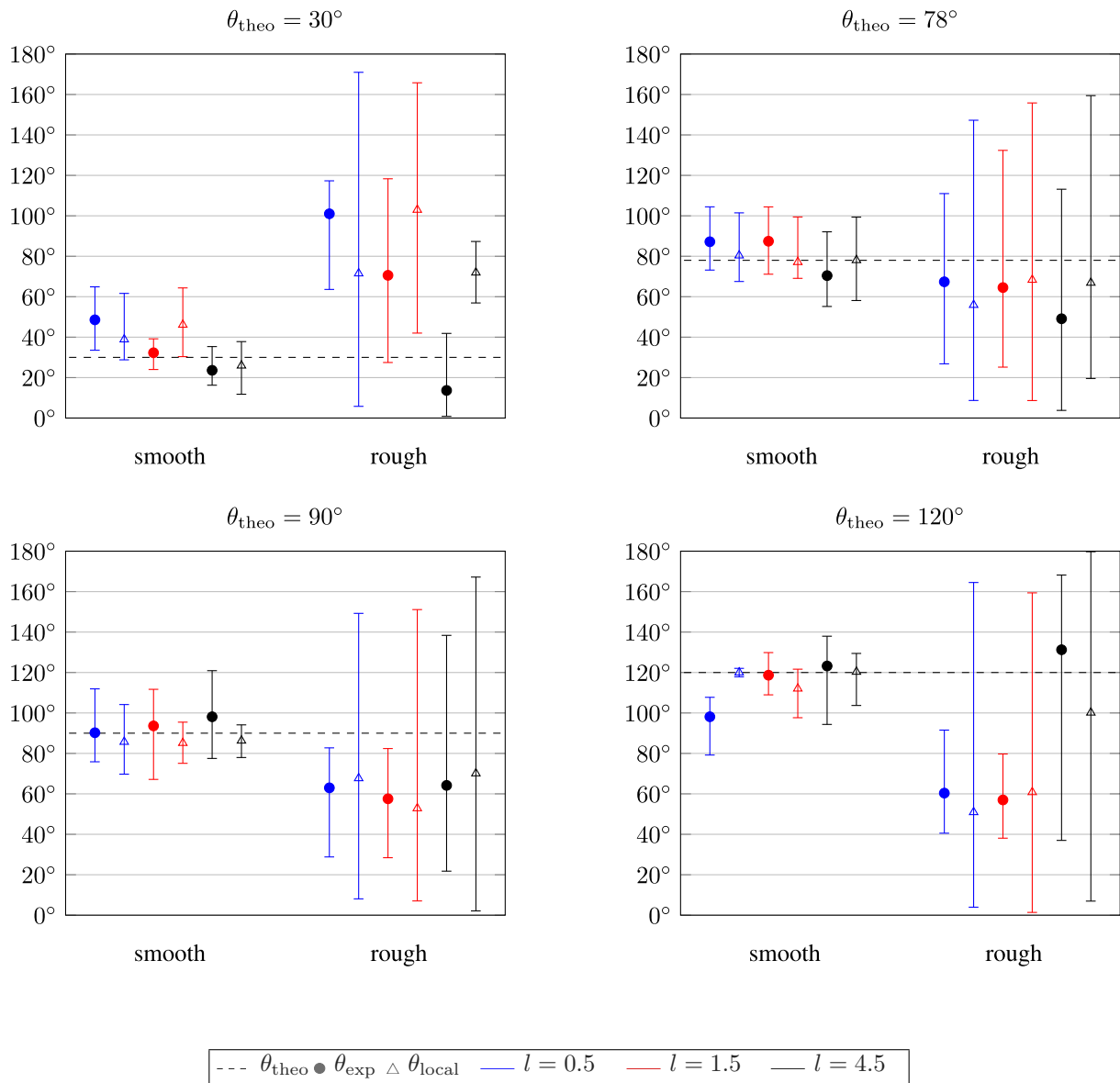
Fig. 5: Mean values of the resulting contact angles θ_{exp} and θ_{local} for simulations with the parameters from Tab. 1.

6   Summary and outlook

In this work, the wetting behavior of rough surfaces was simulated with a phase field model. The qualitative analysis of the results shows a dependence of the behavior on the interface width. However, it was not possible to establish clear tendencies of this behavior. This might be linked to an interference between the relevant length scales. Therefore, further investigations will aim to increase the droplet size in order to decouple it from the other length scales in the simulations. The objective of such investigations is to establish limits for the artificial widening of the interface, as it is done in [11]. This will allow for a switch to more sophisticated phase field models with a relation to real fluid behavior while simulating real rough surfaces with a reasonable effort. In a next step, more advanced roughness models can also be applied. Additionally, dynamic modeling of these scenarios is also of interest.

References

[1] F. Diewald, C. Kuhn, M. Heier, M. Horsch, K. Langenbach, H. Hasse, and R. Müller, PAMM **17**(1), 501–502 (2017).

[2] F. Diewald, M. Heier, M. Horsch, C. Kuhn, K. Langenbach, H. Hasse, and R. Müller, The Journal of Chemical Physics **149**(6), 064701 (2018).

[3] B. Z. Balázs, N. Geier, M. Takács, and J. P. Davim, The International Journal of Advanced Manufacturing Technology **112**(3-4), 655–684 (2020).

[4] J. C. Aurich, M. Bohley, I. G. Reichenbach, and B. Kirsch, CIRP Annals **66**(1), 101–104 (2017).

[5] D. Setti, P. A. Arrabiyeh, B. Kirsch, M. Heintz, and J. C. Aurich, International Journal of Machine Tools and Manufacture **149**(feb), 103489 (2020).

[6] F. Ströer, J. Hering, M. Eifler, I. Raid, G. von Freymann, and J. Seewig, Additive Manufacturing **18**(dec), 22–30 (2017).

[7] M. Heier, S. Stephan, F. Diewald, R. Müller, K. Langenbach, and H. Hasse, Langmuir **37**(24), 7405–7419 (2021).

[8] S. Becker, M. Kohns, H. M. Urbassek, M. Horsch, and H. Hasse, The Journal of Physical Chemistry C **121**(23), 12669–12683 (2017).

[9] M. B. Said, M. Selzer, B. Nestler, D. Braun, C. Greiner, and H. Garcke, Langmuir (2014).

[10] U. Lācis, M. Pellegrino, J. Sundin, G. Amberg, S. Zaleski, B. Hess, and S. Bagheri, Journal of Fluid Mechanics **940**(apr) (2022).

[11] F. Diewald, Phase Field Modeling of Static and Dynamic Wetting, doctoral thesis, Technische Universität Kaiserslautern, 2020.

[12] W. Zhou, J. yuan Tang, Y. fei He, and C. chao Zhu, Journal of Central South University **24**(1), 127–136 (2017).

[13] X. Huang and I. Gates, Scientific Reports **10**(1) (2020).